

Search for Neutrino Tau in the Long Baseline Appearance Experiment

Feng Zhou

8.811 Term Paper

2005-12-16

ABSTRACT

This experiment is designed for the appearance search of $\nu_\mu \rightarrow \nu_\tau$ oscillation in the parameter region indicated by Super-Kamiokande, as the explanation of the zenith dependence of the atmospheric neutrino deficit. The detection is mainly based on the nuclear emulsion technology for the direct observation of the decay of tau leptons produced in ν_τ charged current interactions. The performance of this experiment is compared with the CHORUS experiment.

Contents

1. Introduction

1.1 Physics motivations.....	3
1.2 History Background.....	5
1.2.1 Neutrinos.....	5
1.2.2 Neutrino Oscillation Theory.....	6
1.2.3 Indication of neutrino oscillation.....	7

2. Detector

2.1 Physics requirements and conceptual design.....	14
2.2 The neutrino beam.....	15
2.3 ECC technique.....	17
2.4 Target.....	18
2.5 Electronic trackers.....	19
2.6 Muon spectrometers.....	20

3. Analysis

3.1 Signal detection.....	21
3.2 Selection Criteria.....	22
3.3 Signal estimation.....	23
3.4 Background.....	25

4. Conclusions and outlook..... 28

Reference.....29

Appendix..... 31

Chapter 1

Introduction

1.1 Physics motivations

The neutrinos were introduced in 1932 by W. Pauli to explain the continuous energy spectrum of the electrons emitted in β decay. Since then by means of a large amount of theoretical and experimental work many properties of neutrinos have been determined. They culminated in the neutrino representation inside the Standard Model frame which has been very successful in describing all known neutrino interactions.

Despite of the very positive results many questions remain still unsolved about neutrinos nature. In fact the neutrinos are so weakly interacting particles that it is difficult to obtain measurements with large statistics and high precision. Among all the unsolved questions the more fundamental one is whether or not neutrinos are massive particles. The Standard Model was constructed to give massless neutrino in according to the failure of observing experimentally the right-handed neutrinos. Anyhow it is generally believed that, despite of its spectacular success, the Standard Model is incomplete. Many of its generalizations predict massive neutrino. Also the cosmology strengthens the hypothesis of massive neutrinos. In fact the problem of the nature of the dark matter has, as a possible particle solution, neutrinos with mass value of the order of the electronvolt.

An indirect but very sensitive method to search for non-zero masses is to look at the occurrence of neutrino oscillation, which can happen if neutrinos are massive. The essence of neutrino oscillation is very simple. If neutrinos are massive, it is possible that the mass eigenstates are different from the weak-eigenstates ν_e, ν_μ, ν_τ , i.e.. The neutrino mass matrix in the flavor basis is not diagonal. If this condition is satisfied the weak-eigenstates neutrino produced by the charged current weak-interactions is a linear superposition of different mass eigenstates. During its propagation the different mass states evolve differently so the composition of the initial state in terms of weak states changes with time. This means that the detection of the neutrino through the weak

interactions has non zero probability to reveal a weak state different from the one in which the neutrino has been produced.

In the last 30 years some unexpected experimental observations of the solar and atmosphere neutrinos were interpreted as hints in favor of neutrino oscillation. Moreover in the last a few years, two collaborations, LSND and Superkamiokande, claimed evidences of neutrino oscillation but it is fair to say that the problem is still open.

My experiment is designed to search for $\nu_\mu \rightarrow \nu_\tau$ oscillation with the aim to reach high sensitivity in the Δm^2 for large mixing angle. It is a long baseline appearance experiment which searches for ν_τ in the almost pure ν_μ beam. The ν_τ presence is searched through the charged current reaction $\nu_\tau N \rightarrow \tau X$. Thus the ν_τ detection essentially consists in the τ detection. The τ short lifetime has suggested to use a hybrid detector to distinguish the occurrence of ν_τ CC interactions from the much more frequent ν_μ CC or NC interactions.

1.2 History Background

1.2.1 Neutrinos

The neutrino was introduced by W. Pauli in 1930 to conserve energy in nuclear β decay which required a final state electrically neutral particle with a spin of 1/2 [1]. Anti-neutrinos from reactors were discovered by F. Reines and C. Cowan in 1956 [2] by making use of the reaction $\bar{\nu}_e + p \rightarrow n + e^+$. The positron and electron annihilate, giving two simultaneous photons. The neutron is thermalized until it is eventually captured by a Cadmium nucleus, emitting photons some 15 micro seconds after the positron signal. These delayed coincidence signals were detected and the existence of the neutrino was confirmed. The neutrinos produced in association with muons were observed at the Brookhaven National Laboratory in 1962 [3] and were found not to be the same as those produced in association with electrons. This was the discovery of a second type of neutrino (ν_μ). The tau particle was discovered at the Stanford Linear Accelerator Center in 1975 [4] and its associated tau neutrino was also discovered by DONUT Collaboration in 2000 [5]. The precise measurement of the decay width of the Z boson in e^+e^- collider at LEP constrains the number of light neutrino families to three [6].

In the Standard Model, 12 particles, 6 quarks and 6 leptons, are the constituents of matter. All of these have been discovered experimentally. Each charged lepton (electron, muon, tau) is associated with a neutral lepton or neutrino (ν_e, ν_μ, ν_τ). The quarks are grouped by pairs according to the same rule and so the three generations of leptons and quarks can be written down as follows.

$$\begin{array}{ccc} \begin{pmatrix} \nu_e \\ e \end{pmatrix} & \begin{pmatrix} \nu_\mu \\ \mu \end{pmatrix} & \begin{pmatrix} \nu_\tau \\ \tau \end{pmatrix} & \text{leptons} \\ \begin{pmatrix} u \\ d \end{pmatrix} & \begin{pmatrix} c \\ s \end{pmatrix} & \begin{pmatrix} t \\ b \end{pmatrix} & \text{quarks} \end{array}$$

In the standard model, the neutrino has a zero mass, a zero charge and a spin 1/2.

There is no compelling reason why neutrinos should have zero mass (like the photon), and many experiments have tried to find the neutrino mass directly by measuring the

energy spectrum of tritium β decays. There was no evidence of finite mass, and the upper limit for the ν_e mass is now 3 eV at 95% C.L [7].

There are two minimal modifications of the field content of the Standard Model that can lead to massive neutrinos. First it is possible to add a Higgs triplet, Δ , to the usual doublet to get a term of the form $\nu_L C M \nu_L \Delta$. The non-vanishing vacuum expectation value of Δ gives a Majorana mass and breaks L-conservation. Another possible modification is to assume the existence of ν_R : it would lead to Dirac mass term from the usual Higgs mechanism.

1.2.2 Neutrino Oscillation Theory

Neutrino oscillations take place when physical mass eigenstates ν_i differ from weak eigenstates ν_α , where ν_α is defined to the neutrino state which connects to a charged lepton α via charged current interactions. The weak-eigenstate ν_α can be expressed as a linear superposition of the mass eigenstates ν_i , $\nu_\alpha = \sum_i U_{\alpha i} \nu_i$, where U is a unitary mixing matrix. With three neutrino flavors the mixing matrix can be parameterized by three complex rotations in the following way:

$$U = \begin{pmatrix} 1 & 0 & 0 \\ 0 & c_{23} & s_{23} \\ 0 & -s_{23} & c_{23} \end{pmatrix} \begin{pmatrix} c_{13} & 0 & s_{13}e^{i\delta} \\ 0 & 1 & 0 \\ -s_{13}e^{i\delta} & 0 & c_{13} \end{pmatrix} \begin{pmatrix} c_{12} & s_{12} & 0 \\ -s_{12} & c_{12} & 0 \\ 0 & 0 & 1 \end{pmatrix} \begin{pmatrix} 1 & 0 & 0 \\ 0 & e^{i\phi_1} & 0 \\ 0 & 0 & e^{i\phi_2} \end{pmatrix}$$

where $s_{ij} = \sin(\theta_{ij})$ and $c_{ij} = \cos(\theta_{ij})$. The phases ϕ_1 and ϕ_2 are

Majorana-phases and do not enter into the oscillation probabilities, however they can have phenomenological consequences, e.g. in neutrino-less double beta decay [8]. The CP-phase δ is related to the CP violation effects. The most general parameterization of neutrino mixings can be found in [9].

A mass eigenstate of generation i after a time interval t is given by

$$|\nu_i(t)\rangle = e^{-iEt} |\nu_i(0)\rangle.$$

A neutrino of the generation ν_α after a time interval of t is given by

$$|\nu_\alpha(t)\rangle = \sum_i U_{\alpha i} |\nu_i(t)\rangle = \sum_i U_{\alpha i} e^{-iE_i t} |\nu_i(0)\rangle$$

The time propagation equation of a weak eigenstate neutrino can be written,

$$|\nu_\alpha(t)\rangle = U_{\alpha i} e^{-iE_i t} U_{i\alpha}^\dagger |\nu_\alpha(0)\rangle$$

The general vacuum oscillation probability is then given by

$$P_{\nu_\alpha \rightarrow \nu_\beta} = \left| \langle \nu_\beta | e^{-iE_i t} | \nu_\alpha \rangle \right|^2 = \sum_{ij} U_{\alpha j} U_{\beta j}^* U_{\alpha i}^* U_{\beta i} \exp(-i \frac{\Delta m_{ij}^2 L}{2E})$$

For example, the probability of the oscillation $\nu_\mu \rightarrow \nu_\tau$ is

$$P_{\nu_\mu \leftrightarrow \nu_\tau} = \cos^4(\theta_{13}) \sin^2(2\theta_{23}) \sin^2\left(\frac{1.267 \cdot \Delta m_{23}^2 (eV^2) \cdot L(km)}{E(GeV)}\right)$$

1.2.3 Indication of neutrino oscillation

The first experiment that obtained some hints in favor of neutrino oscillation was a solar neutrino search carried out in the Homestake mine in the early '70. During the last 30 years a large number of experiments strengthened this hypothesis measuring neutrino fluxes from different sources: solar atmospheric, reactor and accelerator. We will briefly discuss the existing experiments.

1. Solar Neutrinos

The major part of the energy of the sun (98%) is produced in the reaction of the thermonuclear pp cycles. Neutrinos are emitted in six reactions of the solar pp cycle: three of these give monochromatic energy lines, the others produce neutrino with continuum spectra (fig.1).

The solar neutrino puzzle started to emerge in the late sixties and it took nearly forty years to resolve it. The first data on solar neutrinos obtained in the Homestake experiment [11] already displayed a difference of roughly a factor of 2:5 between the measured flux and the prediction, albeit at a very low confidence level. The first detection of solar neutrinos was awarded with the Nobel prize in 2002. As more and more data were gathered, the

Figure removed for copyright reasons.

[10] J. N. Bahcall, *Astrophys. J.* 467, 475 (1996).

Fig 1.1 Solar neutrino spectrums [10]

discrepancy between the observed neutrino flux and the theoretically predicted flux increased as it can be seen in figure 1.2[12]. With the advent of the first solar neutrino data from Kamiokande [13] in 1989 the evidence for the solar neutrino deficit was strengthened. This development continued with the first data from Sage [14] in 1991 and from Gallex [15] in 1994. The next major breakthrough in the observation of solar neutrinos was the high quality spectral data delivered by the successor experiment of Kamiokande, Super-K [16], in 1999. The culmination and solution to the solar neutrino puzzle then was achieved by the neutral current data of the SNO experiment in 2002. The neutral current data allow to precisely determine the overall flux of all active neutrino flavors from the Sun and they are found to be in excellent agreement with the predictions. Thus the only possible conclusion is that the electron neutrinos from the Sun undergo a transition to another active flavor. This conclusion can be drawn at the very high confidence level of 5.3σ , i.e. the probability that this result is a statistical fluctuation is approximately 1 in 10^7 . A very detailed description of the impact of the various pieces of evidence and systematical errors is given in [17].

The Kamland experiment, however, provides an independent check of the results of the solar neutrino experiments. Kamland measures the survival probability of electron

anti-neutrinos produced in various nuclear power plants in Japan. This allows a precise test of the solar oscillation hypothesis without any astrophysical uncertainties. The first Kamland data were published in 2002 in [18]. The Kamland result led to a flood of papers analyzing the Kamland data in combination with existing solar data. In all the papers basically the same result was found, namely that the so called MSW-LMA oscillation solution gives the best fit and that any other known mechanism can play at most a sub-leading role in the explanation of the solar neutrino deficit. The remaining parameter ranges derived by a fit to all existing data are at 3σ given by [19]

$$\Delta m_{21}^2 = +7_{-3}^{+23} \cdot 10^{-5} eV^2, \quad \sin^2(2\theta_{12}) = 0.8_{-0.2}^{+0.2}$$

Figure removed for copyright reasons.

[12] J. Bahcall, John Bahcall's homepage, <http://www.sns.ias.edu/~jnb/>.

Fig 1.2 Comparison of the measured and predicted total rates of solar neutrinos[12]

Atmosphere neutrinos

In the Earth's atmosphere neutrinos are produced by reactions of cosmic radiation and the nuclei in the atmosphere. The main components of the cosmic radiation at the relevant energies are protons, which in turn produce via strong interactions mesons. Those mesons are mainly pions and undergo the following decay chain

$$\begin{aligned} \pi^\pm &\rightarrow \mu^\pm + \nu_\mu (\bar{\nu}_\mu) \\ \mu^\pm &\rightarrow e^\pm + \nu_e (\bar{\nu}_e) + \bar{\nu}_\mu (\nu_\mu) \end{aligned}$$

This yields a ratio of muon flavor to electron flavor neutrinos of 2. It was realized in 1960 that the observation of atmospheric neutrinos could be possible using a large water Cherenkov detector deep underground [20]. The ratio of course is not exactly 2 since there are many subtleties involved in the prediction of the atmospheric neutrino flux like the composition of the primary cosmic rays, the incoming flux of particles etc.. However there exist complete models for computing the neutrino flux of each flavor with an accuracy of ~20%. The ratio of electron neutrinos to muon neutrinos is known with a better precision of ~5%, since in the ratio many uncertainties cancel. This ratio has been measured by different experiments. The first generation detectors, which actually were originally designed to search for proton decay, NUSEX, Soudan, IMB Frejus and Kamiokande reported the ration between the measured value and its predicted value based on Monte Carlo simulation. As shown in figure 1.3 [21] some of them measured for R a value smaller than the expected one. The discrepancy between the observed and predicted neutrino flavor ratio is referred to as the atmospheric anomaly. It was considered as a hit in favor of neutrino oscillation.

Figure removed for copyright reasons.

[21] M. C. Gonzalez-Garcia and Y. Nir, Developments in neutrino physics, Rev. Mod. Phys. 75 (2003) 345.

Fig 1.3 Measurement of atmospheric neutrino flavor ratios [21]

Finally in 1998 the Super-K collaboration presented their now famous result atmospheric neutrinos do oscillate. The key to this statement is that Super-K has a sufficient number of events to observe the baseline dependence of the ratio of electron neutrinos to muon neutrinos. The zenith angle distribution of neutrinos is measured as figure 1.4[22]. The zenith angle distribution is the first order of pathlength distribution. When $\cos \theta > 0$ the neutrino comes from the upper hemisphere so it has a pathlength of 15 up to 500Km, whereas the up-going neutrinos ($\cos \theta < 0$) cross the earth so their pathlength is larger, up to 13000Km: thus as $\cos \theta$ increases the distance traveled by neutrinos decreases. Since the neutrino flux is expected to be nearly up-down symmetric, in case of no oscillation the asymmetry should vanish. The ν_e events have an asymmetry compatible with the expectation while ν_μ events show for large momentum a negative asymmetry. In fact for small momentum the oscillation length is small and up and down neutrino experience about the same oscillation probability and reduction. For higher momentum the oscillation length increases so only up-going neutrinos are depleted, therefore an asymmetry appears.

Figure removed for copyright reasons.

[22] Super-Kamiokande Collaboration, A measurement of Atmospheric Neutrino Oscillation Parameters by Super-Kamiokande I, Phys .Rev. D71 (2005) 11.

Fig 1. 4 Zenith angle distribution of ν_μ and ν_e events in Super-K [22]

Supper-K data are very strong evidence in favor of the interpretation of the ν_μ deficit as an effect of neutrino oscillation. It could be $\nu_\mu \rightarrow \nu_e, \nu_\mu \rightarrow \nu_\tau$ or $\nu_\mu \rightarrow \nu_s$. The $\nu_\mu \rightarrow \nu_e$ oscillation seems to be ruled out from the agreement of the ν_e zenith angle and asymmetry distribution with the expectation in case of no oscillation. Moreover since the ν_μ in the 2-flavor model oscillates with nearly maximal mixing angle with Δm^2 in the range 10^{-2} to 10^{-3} eV², the CHOOZ experiment result ruled out the $\nu_\mu \rightarrow \nu_e$ occurrence. The $\nu_\mu \rightarrow \nu_{sterile}$ is also disfavored respect to $\nu_\mu \rightarrow \nu_\tau$ hypothesis by indirect measurement.

The best fit for neutrino oscillation $\nu_\mu \rightarrow \nu_\tau$ from Super-K gives the value

$$\Delta m_{23}^2 = 3.5_{-2}^{+3} \cdot 10^{-3} eV^2, \quad \sin^2(2\theta_{23}) = 1_{-0.2}^{+0}$$

That's the motivation of our experiment.

The CHORUS

The CHORUS (CERN Hybrid Oscillation Research Apparatus) [23] experiment together with NOMAD[24], another CERN experiment which looks for the same phenomena with different techniques on the same neutrino beam line, had been designed to search for $\nu_\mu \rightarrow \nu_\tau$ oscillation with the aim to reach high sensitivity for small mixing angle in the region of large value of Δm^2 . They are the first two short baseline beam experiment searching for the ν_τ appearance.

Since CHORUS's aimed region of oscillation parameters ($\Delta m_{23}^2 \geq 50 - 100 eV^2, \sin^2(2\theta_{23}) \approx 2 \cdot 10^{-4}$) is just on the far away from Super-K allowed region, it's no doubt that after couple years data taking there is no ν_τ candidate found in CHORUS.

But because I will use similar concept of design for my setup, I would like to briefly describe the design of CHORUS.

CHORUS adopts the "hybrid" approach of combining the emulsion and the

electronic detection techniques. The schematic diagram of the CHORUS apparatus is depicted in figure 1.5 [23]. The experimental set-up is composed of an emulsion target, a scintillating fiber tracker system, scintillator trigger hodoscopes, an air-core magnet, a lead/scintillator calorimeter, and a muon spectrometer. The target material consists of a total of 770 kg of nuclear emulsion, where the neutrino interactions are recorded. Reconstruction and analysis of the neutrino events recorded in the emulsion target is carried out by automatic scanning systems. Downstream of the emulsion target are the electronic detectors. The fiber tracker system provides accurate trajectory predictions back to the emulsion target. The good two-track resolution is crucial for event reconstruction. Together with the air-core magnet, the tracker also measures the charge and momentum of the traversing particles. The calorimeter provides high-resolution measurements for the energies and directions of the hadronic and electromagnetic showers, as well as tracking capabilities. The charge and the momentum of the muons are measured by the muon spectrometer system.

Figure removed for copyright reasons.

[23] CHORUS collaboration, A search for $\nu_{\mu} \rightarrow \nu_{\tau}$ oscillation, Phys. Lett. B 424 (1998) 202.

Fig 1.5 CHORUS detector layout [23]

Chapter 2

Detector

2.1 Physics requirements and conceptual design

The basic idea comes from the proposed long baseline neutrino oscillation experiment OPERA [25].

According to the best fit of the data of Super-K, we need to build long baseline experiment to reach the sensitivity of mass difference. The following equation deduced from oscillation probability gives the simple explanation.

$$\Delta m_{23}^2 (eV^2) \approx \sqrt{P} \cdot E(GeV) / (1.27 \cdot L(Km))$$

Therefore, the sensitivity in mass difference depends on the ratio E/L. For a typical accelerator neutrino energy O (10 GeV) we define short-baseline (SBL) experiments as those with L~1 km, so mostly sensitive to $\Delta m_{23}^2 \approx 1 - 10 eV^2$. In order to reach the sensitivity of $\Delta m_{23}^2 \approx 10^{-2} - 10^{-3} eV^2$, long baseline (LBL) experiments where L ~1000 km is required.

In the ν_τ appearance experiment, the signature is the explicit detection of the vertex in the charged-current (CC) interaction $\nu_\tau N \rightarrow \tau X$ and of the subsequent decay topologies, as figure 2.1, of the short-lived tau to its daughters (“kink” for one-prong decays, and “star” for three-prong decays). The principal decay channels of the τ^- which are studied include:

$$\tau^- \rightarrow e \bar{\nu}_e \nu_\tau$$

$$\tau^- \rightarrow \mu \bar{\nu}_\mu \nu_\tau$$

$$\tau^- \rightarrow h^- (n\pi) \nu_\tau$$

with the branching ratio of 17.8%, 17.4% and 49.2%.

Despite its distinctive topology the multi-prong channel of the τ^- has not been

considered due to the less favorable signal to noise ratio.

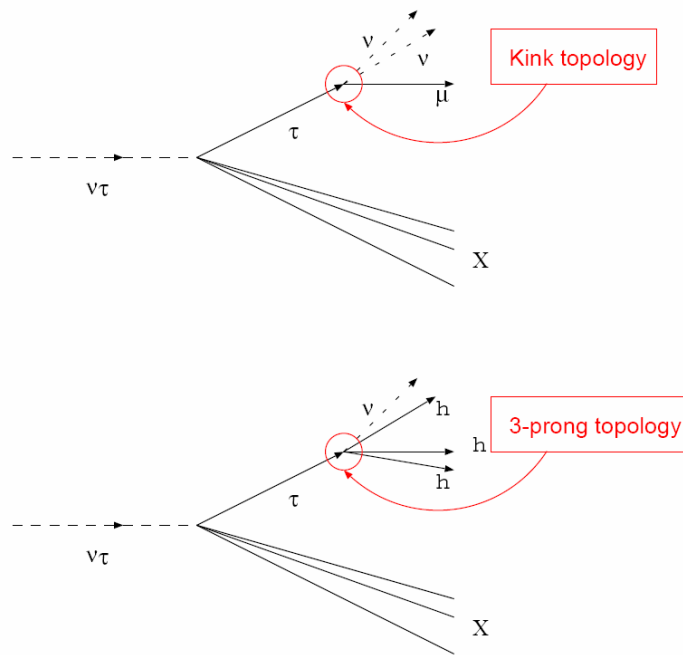


Fig 2.1 Tau decay topologies: 1-prong decay, so-called kink, and 3-prong

2.2 The neutrino beam

For CHORUS, the schematic layout of the WANF is shown in figure 2.2 [26]. Protons extracted from the straight section 6 of the SPS at 450 GeV/C are directed towards the West Experimental Area and focused onto a beryllium target (T9). A fast resonant (FS) extraction is used which produces two beam spills of ~ 6 ms duration, separated by 2.7 s, for each 14.4 s cycle of the accelerator. Pions and kaons produced in the target, in the required energy band, are focused towards the detectors in an approximately parallel beam: two co-axial magnetic lenses, more familiarly known as horn and reflector, are used. These pions and kaons decay in flight to produce muons and muon neutrinos. The muons and remaining hadrons are stopped in a long iron and earth shield at the end of the decay path leaving only the neutrinos to continue to the detectors some 800m from T9. To minimize the number of 'parent' particles that interact in the air before their decay, the spaces between the focusing devices in the 120m long cavern have large-diameter tubes filled with helium at atmospheric pressure.

Figure removed for copyright reasons.

[26] E. Eskut et al, The CHORUS Experiment to search for $\nu_\mu \rightarrow \nu_\tau$ Oscillation, NIM A 401 (1997) 7-44.

Fig 2.2 CHORUS neutrino beam line layout [26]

I plan to use the similar setup to generate the almost pure muon neutrino. The difference is I will use the lower energy protons with higher flux rate. If we run the SPS fully and do not share with other detector like NOMAD, we can surely increase the flux rate of protons.

Comparison of our beam with CHORUS is show on table 2.1

Table 2.1 Comparison of neutrino beam between LBL and SBL experiment

	LBL(mine)	SBL(CHORUS)
Momentum of Proton(GeV/c)	400	450
Total Proton per year	$5 \cdot 10^{20}$	$1 \cdot 10^{19}$
Mean ν_μ energy (GeV)	20	24
ν_μ CC events/year/ton	30	$1.2 \cdot 10^5$
Fraction of other neutrino		
ν_e / ν_μ		0.8%
$\bar{\nu}_\mu / \nu_\mu$		2.2%
$\bar{\nu}_e / \nu_\mu$		0.08%

2.3 ECC technique

I will use the ECC (Emulsion Cloud Chamber) technique which has been successfully applied in DONUT [5](Direct Observation of Neutrino Tau) experiment searching for the ν_τ interactions as illustrated in figure 2.3.

Figure removed for copyright reasons.

[27] B. Lundberg (DONUT Coll.), to appear on the Proc. Of the XIX Int. Conf. on Neutrino Physics and Astrophysics, Sudbury, 2000.

Fig 2.3 Detected Tau event in DONUT [27]

The high position resolution of nuclear emulsion, the existence of automatic readout system and the availability of fast data processing are the essential ingredients of the present ECC detection technique. These techniques have been highly developed in the CHORUS and DONUT experiment.

Nuclear emulsions are made of micro-crystals of silver halides (AgBr) as sensitive devices dispersed in a thin gelatin layer. The size of micro crystal is $\sim 0.2 \mu\text{m}$ and is well controlled by the current industrial technologies for photographic films. Emulsion films have nuclear emulsion layer on both side of a transparent plastic base. We use $50 \mu\text{m}$ thick emulsion layers on both side of a $200 \mu\text{m}$ thick base which is similar as DONUT. This structure of the film allows to connect track segments on both sides of the base. The position and angles of the connected tracks are thus free from distortions in the emulsion layers.

The effort in developing automatic systems for the analysis of nuclear emulsions was initiated by Niwa in the late 70's [28]. The concept proposed at that time of fully automatic track reconstruction is still the basic algorithm in the recent systems. In order to recognize the presence of tracks penetrating almost perpendicularly the emulsion layer, a series of digitized tomographic images are recorded through the emulsion depth. The correlation of grains in the different layers identifies the track segments.

For each emulsion layer positions and angles of the detected tracks are recorded as micro tracks. Then, the micro tracks on the two sides of the base are connected to form base tracks, whose positions and angles are not affected by distortion. After collecting these base tracks in a series of emulsion film, track reconstruction is performed. In DONUT the deviation of the measured micro track positions from the reconstructed line is $\sim 0.3 \mu\text{m}$. This resolution, mainly determined by the precision of the readout system, is perfectly adequate for the detection of tau decays.

The emulsion structure is also well suited for the measurement of charged particle momenta and for particle identification. The momentum is measured from the multiple scattering. Electrons can be identified by detecting cascade electromagnetic showers. Gamma rays are detected by their conversion into electron pairs. The total energy of electrons and gammas can be evaluated by the analysis of the shower development.

The above features have been exploited in the DONUT analysis and will be applied in my long baseline experiment.

The whole detector is composed of 3 same modules. Each module is made of 30 stations interleaved by electronic trackers, and one muon spectrometer. Total target mass of 5500 ton can be reached by this design.

2.4 Target

Since it's a long baseline neutrino experiment, I need a huge and massive target. Bulk emulsion model can not reach the desired mass. I should use the ECC model as described above. The difference with DONUT is I will use lead instead steel because of its larger density.

The basic structure of one station is obtained by stacking 50 1mm thick lead plates interleaved with thin emulsion films. Each film has 50 μ m thick emulsion layers on both side of a 200 μ m thick plastic base. The thickness of one station is about 10 radiation length which is enough to allow electron identification through their electromagnetic showering and momentum measurement by multiple scattering. The basic structure and neutrino tau interaction topology is showed on figure 2.4.

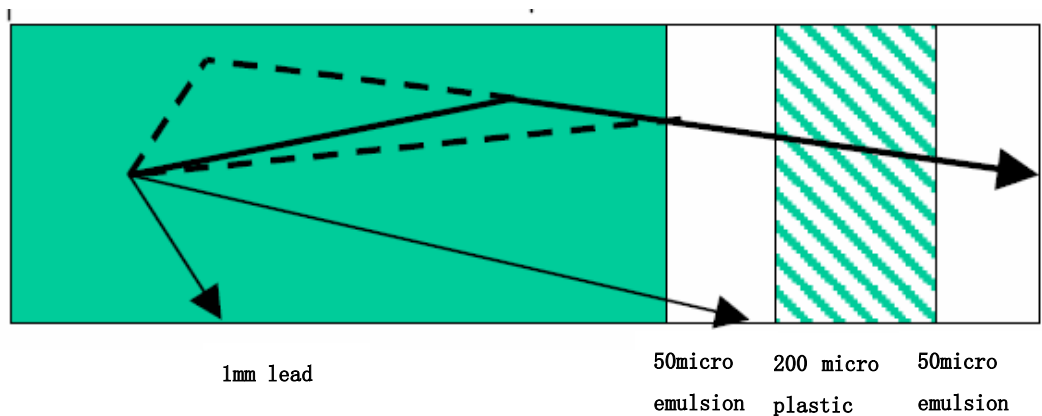


Fig 2.4 Basic structure of emulsion module and topology of tau decay

Each station has transverse dimensions of $10 \times 10 \text{ m}^2$. Since it's impossible to scan the whole station whenever we find neutrino CC interaction, we will separate each station into small bricks with transverse dimension of $10 \times 10 \text{ cm}^2$. The electronic trackers will be used to locate the brick where the neutrino CC interaction happens.

2.5 Electronic trackers

The required spatial resolution of the electronic tracker is determined by the need of a high brick location efficiency. For DONUT, it uses fiber scintillators to locate the primary vertex to greatly reduce the heavy burden of emulsion scan. In my design the plastic scintillator strips with diameter of 1cm is enough to locate the brick. The read out of scintillator is coupled to photodetectors by wavelength shifting fibers. The same technique has been used for MINOS experiment [29].

So the basic design is each station is followed by two electronic tracker planes (with

strips oriented along X and Y axis respectively). Each planes covers area by $10 \times 10 \text{m}^2$ with total 1000 10 meter long strips. The electronic tracker also acts as trigger. Whenever the two planes are both hit and deposited certain amount energy, the downstream trackers and muon spectrometers are triggered to take data.

The located brick will be removed for scan. If possible tau candidate is found, the downstream and adjacent bricks will be removed for full scan. New bricks will be filled in.

2.6 Muon spectrometers

Muon spectrometers are built to measure the charge and momentum of muons. It can help to locate the vertex and reject the background from ν_μ CC interactions. Each muon spectrometer consists of an analysis magnet and high resolution trackers. Drift chambers are arranged before, in and after the magnet as high resolution trackers. The detail can be found in the DONUT experiment except we need to build huge magnet field with transverse dimension of $12 \times 12 \text{m}^2$ for muon acceptance.

The layout of the whole detector is showed on figure 2.5

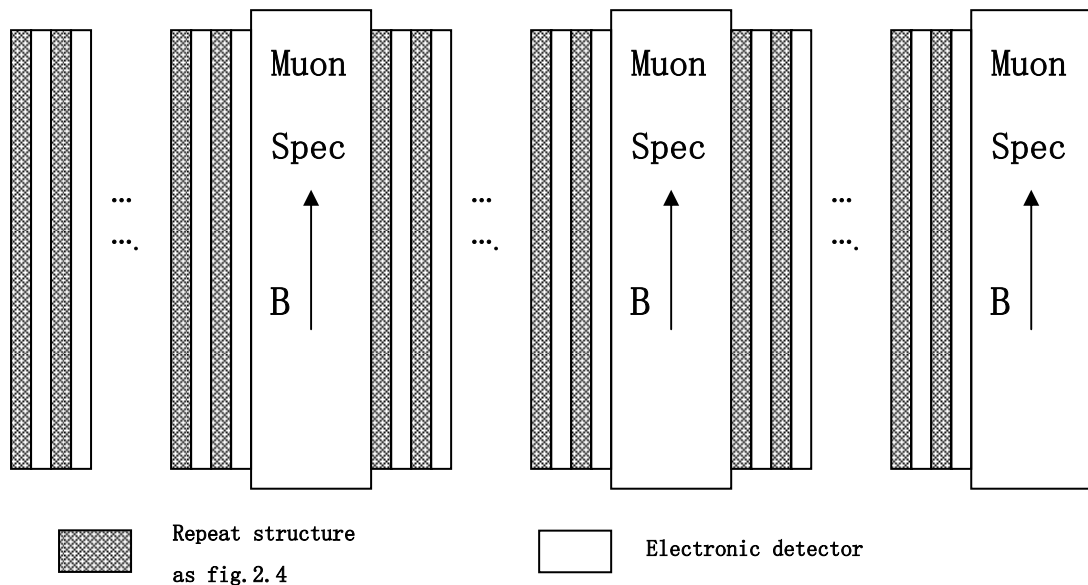


Fig 2.5 Layout of the detector

Chapter 3

Analysis

3.1 Signal detection

As we mentioned in 2.1, the ν_τ signature is the explicit detection of the vertex in the charged-current (CC) interaction $\nu_\tau N \rightarrow \tau X$ and of the subsequent decay topologies of the short-lived to its daughters (“kink” for one-prong decays). The principal decay channels of the τ^- which are studied include:

$$\tau^- \rightarrow e \bar{\nu}_e \nu_\tau$$

$$\tau^- \rightarrow \mu \bar{\nu}_\mu \nu_\tau$$

$$\tau^- \rightarrow h^- (n\pi) \nu_\tau$$

In our ECC model, if a tau is produced in a lead plate it will decay either in the same plate (short decay) or further downstream (long decay), which is shown in figure 3.1.

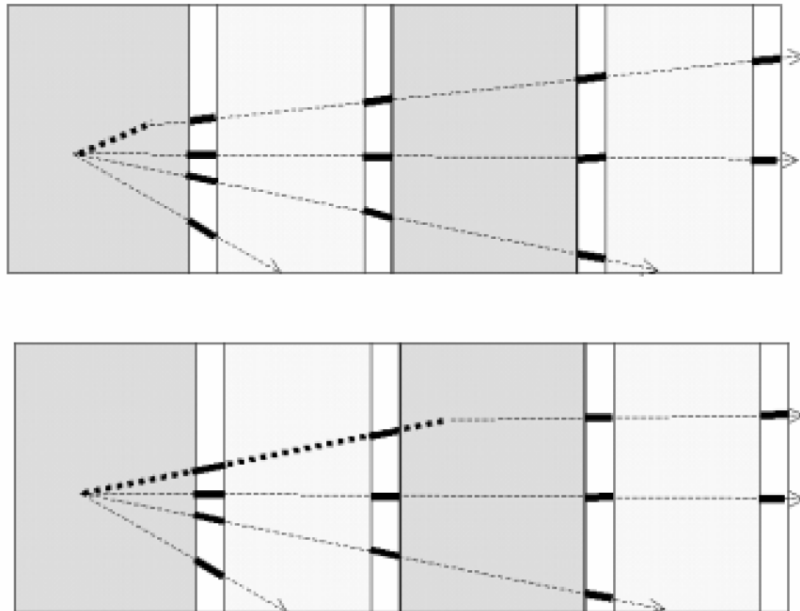


Fig 3.1 Schematic of short (top) and long (bottom) tau decays.

For long decay, the tau is detected by measuring the angle between the charged decay daughter and the parent direction. For the measurement the directions of the tracks before and after the kink are reconstructed by means of the pair of emulsion films sandwiching the lead plate where the decay vertex occurred. A fraction of the short decays is detectable by measuring a significant impact parameter (IP) of the daughter track with respect to the tracks originating from the primary vertex.

The detection of the tau decay into an electron benefits from the dense brick structure, which allows electron identification through its showering in the downstream layers.

For the muonic decay mode the presence of the penetrating muon track allows an easier event vertex finding. The potential background from large angle scattering of muons produced in ν_μ CC interactions can be reduced to a tolerable level by applying cuts on the kink angle and on the transverse muon momentum at the decay vertex.

Hadronic decay modes have the largest branching ratio but are affected by background due to hadron reinteractions. One of the primary hadrons, in fact, can interact in the first lead plates and, if the other products of this interaction are not detected in the emulsion, it may simulate the charged single-prong decay of the tau. Strong kinematical cuts can be used to reduce this background.

An important tool for background rejection is the determination of the transverse momentum of the daughter particle with respect to the direction of the tau track candidate. For electronic tau decays the ECC technique is well suited to identify electrons and to determine their energy by measuring the density of track segments associated to their showering in the brick. For charged hadrons and muons, the momentum is deduced from the measurement of the multiple scattering in the lead plates. As discussed above, the muon momentum is also measured by the muon spectrum meter in a large fraction on the cases.

3.2 Selection Criteria

The criteria of selection from DONUT and CHORUS are listed as following, some parameters are adjusted according to the lower energy in my experiment compared to

DONUT.

1. None of the tracks originating at the primary interaction vertex was identified as a muon or electron.
2. Only one daughter track was associated with a parent track.
3. The parent track was < 1 mm long.
4. The daughter angle with respect to the parent track was >10 mrad and < 400 mrad.
5. The impact parameter of the daughter to the parent track was $< 10 \mu\text{ m}$.
6. The impact parameter of the parent track to the interaction vertex was $< 10 \mu\text{ m}$.
7. The daughter track momentum was > 1 GeV/C for electron and muon, >2 GeV/C for hadron.
8. The transverse momentum of the decay was >250 MeV/c.
9. For short decay, the impact parameter of the daughter track to the primary vertex was $> 10 \mu\text{ m}$ and $< 500 \mu\text{ m}$. The muonic decay mode is not considered in short decay because of its high background from muon multiple scattering.

3.3 Signal estimation

According to the above selection criteria, total 10% of the detection efficiency (\times Branching Ratio) can be achieved.

The number of ν_τ interactions in my detector is determined by the following formula:

$$N_\tau = A \int \left(\phi_{\nu_\mu}(E) \times P_{\nu_\mu \rightarrow \nu_\tau}(E) \times \sigma_{\nu_\tau}(E) \times \varepsilon_{\text{detection}} dE \right)$$

where $\phi_{\nu_\mu}(E)$ is the flux at the detector site, $P_{\nu_\mu \rightarrow \nu_\tau}(E)$ is the oscillation probability between ν_μ and ν_τ , $\sigma_{\nu_\tau}(E)$ is the ν_τ CC interaction cross-section, $\varepsilon_{\text{detection}}$ is the tau detection efficiency, A is the number of nucleons in the effective detector mass.

In case the condition $\frac{1.267 \cdot \Delta m_{23}^2 (eV^2) \cdot L(km)}{E(GeV)} \ll 1$ holds, the oscillation

probability can be approximated as follows:

$$P = \sin^2(2\theta_{23}) \left(\frac{1.267 \cdot \Delta m_{23}^2 (eV^2) \cdot L(km)}{E(GeV)} \right)^2$$

Moreover, the ν_τ cross-section can be parameterized as:

$$\sigma_{\nu_\tau} = \sigma_0 \times E$$

where $\sigma_0 = 0.67 \times 10^{-42} m^2$. Then the number of ν_τ interactions may be expressed

as:

$$N_\tau = A \times \sin^2(2\theta_{23}) \left(1.267 \cdot \Delta m_{23}^2 (eV^2) \cdot L(km) \right)^2 \times \sigma_0 \times \varepsilon_{\text{detection}} \times \int \left(\phi_{\nu_\mu}(E) dE / E \right)$$

For CHORUS, the ν_μ flux is simulated by MC as figure 3.2.

Figure removed for copyright reasons.

[26] E. Eskut et al, The CHORUS Experiment to search for $\nu_\mu \rightarrow \nu_\tau$ Oscillation, NIM A 401 (1997) 7-44.

Fig 3.2 Neutrino flux composition and distribution [26]

My ν_μ flux has the similar shape except the flux rate is approximate $5 \cdot 10^{-5}$ smaller.

Considering the following parameters,

Total mass of the target: 5.5kton and 7000 times of CHORUS

Length of base line: 1000meters

Mean energy of ν_μ flux: $E=20\text{GeV}$

Range of mass difference: $\Delta m_{23}^2 = 10^{-3} - 10^{-2} eV^2$

Large mixing angle: $\sin^2(2\theta_{23}) = 1$

Running time: 5years

The total number of detected tau could be $\sim 10^2 - 10^3$ and ~ 300 for best fit value

$$\Delta m_{23}^2 = 3.5 * 10^{-3} eV^2.$$

The total neutrino interactions could be $4 * 10^5$ (including all neutrino flavors and NC events).

3.4 Background

The main background sources are

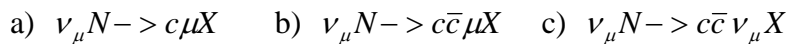
1. prompt ν_τ production in the primary proton target and in the beam dump

Prompt ν_τ originate from the decay of tau's produced by the decay of D_s mesons.

Similarly as CHORUS, the number of ν_τ CC interactions per ν_μ CC interaction has been estimated to be $\sim 3-4 * 10^{-6}$. The contribution to the background is completely negligible if one also takes into account of detection efficiency.

2. one-prong decay of charmed particles

Charmed particles are produced in CC and NC neutrino interactions through the reactions



These processes may constitute a background if one fails to detect the primary muon (a,b) or the charm partner (b,c). The most relevant source is given by single charm production (a), since charmed mesons have masses and lifetimes similar to those of the tau. If the primary muon is missed, a D^+ meson decaying in one charged particle can fake a genuine tau event, since the positive sign of the D^+ daughter is only measured for the

muonic channel by the muon spectrometers.

3. background from π^0 and prompt electrons

In addition to charm production, two other source must be considered as possible background for $\tau \rightarrow e$ decays: kink-like events from scattering of primary electrons produced in ν_e CC interactions and pion charge exchange process ($\pi^- p \rightarrow \pi^0 n$) in ν_μ NC interactions.

4. large angle muon scattering

Muons produced in ν_μ CC events and undergoing a scattering in the lead plate following the vertex plate could mimic a muonic tau decay. The cut of transverse momentum and kink angle will greatly reject this background.

5. hadronic reinteractions

An important source of background to the hadronic decay channel is due to reinteractions in the lead of hadrons produced in ν_μ NC and ν_μ CC interactions in which the primary muon is not identified. Hadron reinteractions can also contribute to the $\tau \rightarrow \mu$ channel when a hadron, produced either in ν_μ NC or ν_μ CC interactions with the muon not identified, is misidentified as a muon.

All above background sources have been estimated by analysis of CHORUS.

Table 3.1 Summary of expected background for 0 μ (up) and 1 μ (down) sample [30]

Figure removed for copyright reasons.

[30] Alessia Satta, Analysis of the Nu_mu->Nu_tau oscillation search in the CHORUS experiment, PhD Thesis, Rome University.

The ratio of total background to the number of neutrino interactions are estimate lower than $5 \cdot 10^{-5}$. Multiplied by the total neutrino interactions in 5 year running time, $4 \cdot 10^5$, the total number of background is estimated to be less than 20 events. Compared with the signal ~ 300 events, the goal of this experiment can be achieved.

Chapter 4

Conclusions and outlook

In this document, a long baseline experiment searching for ν_τ appearance is discussed. The experiment design is based on the Emulsion Cloud Chamber (ECC) detector, a modular structure made of a sandwich of passive material plates interspaced with emulsion layers. By assembling a large quantity of such modules, one can realize a ~ 5.5 kton fine-grained vertex detector optimized for the study of ν_τ appearance.

Thanks to Prof. Chen, CR-39 is suggested to replace the emulsion as alternative technology solutions. CR-39 is a polymer ($C_{12}H_{18}O_7$) with a density of ~ 1.3 g/cm³. When a charged particle crosses the detector surface it causes radiation damage along trajectory. This zone of structure damage may be increased to $10^{-4} - 10^{-2}$ cm by etching in a chemical reagent. The etching ratio depends on the energy deposition of particles.

$$V = V_T/V_B = f(dE/dx)$$

where dE/dx is stopping power of particle, V_T and V_B are track and bulk etch rates respectively. So by using the CR-39, we can not only reach the space resolution of a few micros but also get more information of particles like momentum. But technique demands some special conditions, such as purification of detector surface and correct calibration procedure etc., deeper investigation should be done to properly apply CR-39 to ν_τ detection.

Reference

- [1] W. Pauli, Letter to L.Meitner and her colleagues (letter open to the participants of the conference in Tübingen (1930).
- [2] F. Reines and C. L. Cowan, Nature 178, 446 (1956).
- [3] G. Danby et al., Phys. Rev. Lett. 9, 36 (1962).
- [4] M. L. Perl et al., Phys. Rev. Lett. 35, 1489 (1975).
- [5] K. Kodama et al. [DONUT Collaboration], Phys. Lett. B 504, 218 (2001)
- [6] t. L. Group and t. S. Group [OPAL Collaboration], arXiv:hep-ex/0212036.
- [7] V. M. Lobashev et al., Phys. Lett. B 460, 227 (1999).
- [8] B. Kayser, ν_{τ} , ν_{μ} , and ν_{e} phases and their effects in Majorana particle processes, Phys. Rev. D30 (1984), 1023.
- [9] J. Schechter and J. W. F. Valle, Neutrino masses in $SU(2)_U(1)$ theories, Phys. Rev. D22 (1980), 2227.
- [10] J. N. Bahcall, Astrophys. J. 467, 475 (1996)
- [11] J. Davis, Raymond, D. S. Harmer, and K. C. Hoffman, Search for neutrinos from the Sun, Phys. Rev. Lett. 20 (1968), 1205-1209.
- [12] J. Bahcall, John Bahcall's homepage, <http://www.sns.ias.edu/~jnb/>.
- [13] Kamiokande-II, K. S. Hirata et al., Observation of solar neutrinos in the Kamiokande-II detector, Phys. Rev. Lett. 63 (1989), 16.
- [14] Sage, V. N. Gavrin et al., First measurement of the integral solar neutrino flux by the Soviet-American Gallium experiment (Sage), (1991), Given at 11th Moriond Workshop: Tests of Fundamental Laws in Physics, LesArcs, France, 26 Jan - 2 Feb 1991.
- [15] Gallex, P. Anselmann, Gallex results from the first 30 solar neutrino runs, (1994), Prepared for 29th Rencontres de Moriond: Electroweak Interactions and United Theories, Meribel les Allues, France, 12-19 Mar 1994.
- [16] Super-K, M. B. Smy, Solar neutrinos with Super-Kamiokande, Phys. Rev. Lett. 65 (1999), 1297-1300, hep-ex/9903034.
- [17] G. L. Fogli, E. Lisi, A. Marrone, D. Montanino, and A. Palazzo, Getting the most

- from the statistical analysis of solar neutrino oscillations, Phys. Rev. D66 (2002), 053010, hep-ph/0206162.
- [18] Kamland, K. Eguchi et al., First results from Kamland: Evidence for reactor anti-neutrino disappearance, Phys. Rev. Lett. 90 (2003), 021802, hep-ex/0212021.
- [19] V. Barger and D. Marfatia, Kamland and solar neutrino data eliminate the low solution, Phys. Lett. B555 (2003), 144-146, hep-ph/0212126.
- [20] M. A. Markov and I. M. Zheleznykh, On high energy neutrino physics in cosmic rays, Nuclear Physics 27 (1961), 385. K. Greisen, Cosmic ray showers, Ann. Rev. Nucl. Science 10 (1960), 63.
- [21] M. C. Gonzalez-Garcia and Y. Nir, Developments in neutrino physics, Rev. Mod. Phys. 75 (2003), 345
- [22] Super-Kamiokande Collaboration, A measurement of Atmospheric Neutrino Oscillation Parameters by Super-Kamiokande I, Phys.Rev. D71 (2005) 112005
- [23] CHORUS collaboration, A search for $\nu_{\mu} \rightarrow \nu_{\tau}$ oscillation, Phys. Lett. B 424 (1998) 202.
- [24] The NOMAD Collaboration, THE NOMAD EXPERIMENT AT THE CERN SPS, CERN PPE/97-059
- [25] H. Pessard, The OPERA Experiment, Physica Scripta. Vol. T93, 59-64, 2001
- [26] E. Eskut et al, The CHORUS Experiment to search for $\nu_{\mu} \rightarrow \nu_{\tau}$ Oscillation, NIM A 401 (1997) 7 -44
- [27] B. Lundberg (DONUT Coll.), to appear on the Proc. Of the XIX Int. Conf. on Neutrino Physics and Astrophysics, Sudbury, 2000
- [28] K. Niwa et al., Proc. Int. Cosmic Ray Symp. On High Energy Phenomena (Cosmic Ray Lab., Univ. Tokyo, 1974) 149.
- [29] E. Ales et al., Fermilab Proposal P-875 (1995); NuMI-L-337 (1998).
- [30] Alessia Satta, Analysis of the $\nu_{\mu} \rightarrow \nu_{\tau}$ oscillation search in the CHORUS experiment, PhD Thesis, Rome University.
- [31] K. Kodama et al. [DONUT Collaboration], Detection and analysis of tau - neutrino interactions in DONUT emulsion target NIM A 493 (2002) 45 - 66

Appendix

Momentum measurement by Multiple Coulomb Scattering

The momentum of a charged particle can be measured from its multiple coulomb scattering in the ECC bricks. The basic unit for measurement is one lead plate 1 mm thick sandwiched by two emulsion films. One brick has 50 layers and thus about 100 independent measurement of the track angle in two projections can be obtained for each passing track.

When a particle of momentum p and velocity βc transverses a material of thickness X measured in units of radiation length (for 1 mm lead plate $X=1/5.6$) the distribution of the scattering angle in a plane is approximately Gaussian with a RMS given by

$$\theta_0 = \frac{13.6 \text{ MeV} / c}{p\beta} \sqrt{X}$$

I will mainly discuss the Coordinate Method used in DONUT [31].

A schematic overview of the principle of the MCS method is shown in figure A.1.

Figure removed for copyright reasons.

[31] K. Kodama et al. [DONUT Collaboration], Detection and analysis of tau neutrino interactions in DONUT emulsion target NIM A 493 (2002) 45–66.

Fig A. 1 Schematic figure of the momentum measurement by using the information of MCS [31]

The root mean square of the position displacement in one projection (y) is expressed as $y_{rms} = \sqrt{\langle y^2 \rangle} = \sqrt{\frac{2}{3}} \times k / p\beta \times \sqrt{X} \times t$ where k is the scattering constant and t is the thickness of the material.

The y_{rms} has $t^{3/2}$ dependence from MCS, but the measurement error is independent of t . This dependence allowed the measurement of higher momentum particles by increasing t so that the displacement was observable. It should be noted that a good plate-by-plate alignment procedure was indispensable for this measurement.

The measured y_{rms} , y_{rms}^{meas} , was the addition of the y_{rms} from MCS and the measurement error ϵ_y : $y_{rms}^{meas} = \sqrt{y_{rms}^2 + \epsilon_y^2}$. Since ϵ_y was measured in the alignment sequences, one could estimate the y_{rms} confidently. The distribution of y was described by a Gaussian distribution to a good approximation. The momentum of a track was extracted from the measured standard deviation, with the accuracy $\Delta y_{rms} / y_{rms}$ expressed as $1/\sqrt{2n}$, where n was the number of independent measurements. If 11 independent position measurements were used, giving 10 displacements, the error was 22%.